Article:

Lu, H. orcid.org/0000-0003-2777-3321, He, L. orcid.org/0000-0002-2537-2244, Gilbert, M. orcid.org/0000-0003-4633-2839 et al. (1 more author) (2025) Plastic layout optimization of hybrid truss and beam structures. Structural and Multidisciplinary Optimization, 68 (3). 54. ISSN 1615-147X

https://doi.org/10.1007/s00158-025-03986-0

Structural and Multidisciplinary Optimization (2025) 68:54
https://doi.org/10.1007/s00158-025-03986-0

RESEARCH PAPER

Plastic layout optimization of hybrid truss and beam structures

Hongjia Lu[1] · Linwei He[2] · Matthew Gilbert[2] · Andrew Tyas[2]

Received: 25 October 2024 / Revised: 30 January 2025 / Accepted: 17 February 2025

Abstract

Classical layout optimization is a well-established structural design tool, however it considers only truss structures composed solely of axially loaded bars, limiting its applicability to many structures. To address this limitation, this study introduces a novel approach that takes into account moment-resisting beams in the optimization framework. The interaction between moment, shear, and axial forces is simplified for inclusion in the optimization problem, solved effectively via a sequential conic programming scheme. Various numerical examples show that the proposed approach identifies structures with lower-volume than the classical layout optimization in problems involving multiple load cases or pre-existing members. Additionally, the method can also be used to solve problems that classical layout optimization cannot address, including constrained design spaces and point moment loads. The findings indicate that the proposed approach provides greater flexibility and efficiency in designing hybrid truss and beam structures, paving the way for versatile structural solutions.

Keywords Truss layout optimization · Beam structure · Multiple load cases · Sequential conic programming

1 Introduction

Beams are essential structural elements widely employed in civil infrastructure, including bridges, tunnels, and buildings. Unlike truss bars, which primarily resist axial forces, beam elements provide moment resistance capabilities, allowing greater flexibility in load transmission and enabling more regularized structural layouts. Consequently, the mechanical performance of beam elements has been extensively studied, and modern design codes offer detailed guidance for their design. However, determining the overall structural layout heavily relies on engineering expertise, which is labour-intensive and may lead to suboptimal solutions. To address this, this study uses an optimization approach to automate the design of structural layouts that incorporate beam elements.

Responsible editor: Qing Quan Liang

✉ Linwei He
linwei.he@sheffield.ac.uk

[1] Future City (Intelligent Industrial Construction) Laboratory, Innovation Center of Yangtze River Delta, Zhejiang University, Jiaxing 314100, China

[2] School of Mechanical, Aerospace and Civil Engineering, University of Sheffield, Mappin Street, Sheffield S1 3JD, UK

One pioneering work of the layout optimization approach is based on the 'ground structure' discretization proposed by Dorn et al. (1964), which identifies (near) optimal truss structures. While this method yields structurally efficient structures, it assumes that the members carry only axial forces, often resulting in complex solutions that are impractical for real-world engineering applications. To address these limitations, subsequent studies have developed various approaches to identify efficient and simpler structures comprised beam members. These approaches can be broadly classified into three distinct categories.

The first category focuses on employing meta-heuristic approaches to identify beam structures that satisfy various practical engineering constraints. For example, Hasançebi et al. (2010) utilized the simulated annealing algorithm to identify efficient beam structures that satisfy strength capacity requirements defined by practical design codes. Liu et al. (2012) used a genetic algorithm to optimize beam structures under structural frequency constraints. Gholizadeh and Ebadijalal (2018) employed a performance-based update scheme to identify the optimized arrangement of brace elements for beam structures. Other notable approaches include the use of the particle swarm algorithm (Esfandiari et al. 2018), the Harmony search algorithm (Bekdaş et al. 2022) and the Bang-big crunch algorithm (Camp and Huq 2013). Meta-heuristic approaches are particularly effective

Published online: 27 March 2025

for tackling complex structural problems where the gradient information is difficult to obtain. Nevertheless, as suggested by Sigmund (2011), meta-heuristic approaches are often associated with high computational costs. Consequently, the target problem is typically 'size optimization' rather than 'layout optimization'.

The second category utilizes gradient-based update schemes and focuses on minimizing structural compliance (i.e., 1/stiffness) with a given amount of material. One of the early research was carried out by Steven et al. (2000), who used a stress-based criterion to iteratively update member cross-sectional areas, thereby enhancing structural stiffness. Later Pedersen (2003) extend this approach to consider material and geometrical non-linearities; Takezawa et al. (2007) incorporated the design of cross-sectional shapes; and Changizi and Jalalpour (2017, 2018); Ahmadi et al. (2018); Changizi and Warn (2020) included stability and uncertainty constraints. In order to reduce the complexity of beam structures, Fredricson (2005) considered the penalty of joints by including micro ground structures and Shen and Ohsaki (2020) carried out geometry optimization with a force density approach. In order to reduce the numerical cost of the beam structure optimization, Li and Chen (2010) proposed a new approach, constructing the ground structure with node positions selected based on the principal stress lines from finite element analysis. To address the problem of multiple load cases, Zhang et al. (2017) used a stochastic sampling approach to cope with a large number of load cases. Tyburec et al. (2021) employed a semidefinite programming formulation to identify globally optimal beam structures, but the high computational complexity makes it suitable only for small-scale problems. Ma et al. (2023) employed a post-processing approach to extract the skeleton from the continuum topology optimization results. Habashneh and Rad (2024) incorporated geometric and material nonlinearities into topology optimization of an I-section beam, enhancing material utilization by accounting for its plastic deformation capacity. These studies can effectively lead to high stiffness structure. However, stress constraints are often excluded due to the significant computational costs they can incur when used in conjunction with the ground structure discretization approach.

The third category is rooted in classical plastic layout optimization, which employs the ground structure approach and assumes rigid-plastic material behaviour. With this material assumption, structural optimization problems can be formulated to generate minimum-weight designs under stress constraints (e.g., Gilbert and Tyas 2003; He and Gilbert 2015; He et al. 2019). Unlike classical topology optimization methods, such as the Solid Isotropic Material with Penalization (SIMP) method, plastic layout optimization formulates the problem as a linear programming model. This formulation utilizes modern interior point solvers, resulting in lower computational costs while ensuring globally optimal solutions. Consequently, plastic layout optimization is especially well-suited for generating benchmark solutions in large-scale problems. However, surprisingly little work has been done to include beams in layout optimization using plastic assumptions. A grillage layout optimization method was introduced by Bolbotowski et al. (2018). However, in this work, the beams were under pure bending, with no allowance for axial forces, and shear failure was also neglected.

Therefore, this study seeks to extend the classical plastic layout optimization approach by incorporating moment-resisting members, enabling the method to address problems involving moment loads and constrained design spaces. To achieve this, new assumptions are introduced to automatically account for the interaction between shear force, axial force, and moment during the design stage. Additionally, a sequential conic programming scheme is implemented to efficiently solve the optimization problem. The remainder of the paper is structured as follows: Sect. 2 reviews classical layout optimization formulation and introduces the new beam-and-truss optimization approach; Sect. 3 presents a few numerical examples; Sect. 4 includes relevant discussions and Sect. 5 concludes the findings.

2 Theory

This section begins with a review of the classical layout optimization method, followed by the introduction of the new formulation for optimizing hybrid beam-and-truss structures. Additionally, a geometry optimization method is presented, which further improves optimization solutions by refining nodal positions in a post-processing step.

2.1 Classical layout optimization approach

The main steps in classical 'numerical' layout optimization, which utilizes the ground structure approach, are shown in Fig. 1. Firstly, the pre-defined design domain is discretized into a nodal grid (Fig. 1a). Secondly, the ground structure, which contains all possible members connecting every pair of nodes, is created (Fig. 1b). Thirdly, the optimal subset of the ground structure is identified (Fig. 1c) by solving the optimization problem shown in Equation (1) [after Gilbert and Tyas (2003) and He and Gilbert (2015)].

$$\min_{\mathbf{a},\mathbf{q}} \quad V = \mathbf{l}^{\mathrm{T}}\mathbf{a}, \tag{1a}$$

$$\text{subject to} \quad \left.\begin{aligned} &\mathbf{B}\mathbf{q}^{\alpha} = \mathbf{f}^{\alpha}, &(1b)\\ &-\boldsymbol{\sigma}^{-}\mathbf{a} \le \mathbf{q}^{\alpha} \le \boldsymbol{\sigma}^{+}\mathbf{a}, &(1c)\end{aligned}\right\}\forall\alpha$$

$$\mathbf{a} \ge \mathbf{0}, \tag{1d}$$

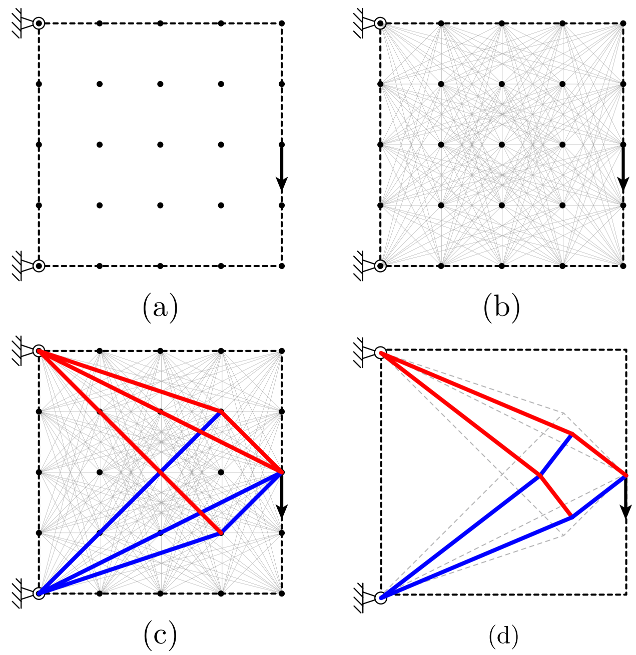

Fig. 1 Four steps of the layout optimization approach: **a** discretize the design domain into a node grid; **b** build the ground structure which includes every possible interconnection between the nodes; **c** use the layout optimization formulation to select the optimal subset structure from the ground structure; **d** rationalize the structure with geometry optimization (red and blue bars represent structural elements in tension and compression, respectively)

where $\alpha = 1, 2, ..., M$ represents the load case index, and M denotes the number of load cases; V is the total structural volume; $\mathbf{B}$ is a $2n \times p$ equilibrium matrix, with n and p denoting the number of nodes and members, respectively; $\mathbf{a} = [a_1, a_2, ..., a_p]^{\mathrm{T}}$, $\mathbf{l} = [l_1, l_2, ..., l_p]^{\mathrm{T}}$ are vectors containing cross-sectional areas and lengths of members; $\mathbf{q}^\alpha = [q_1^\alpha, q_2^\alpha, ..., q_p^\alpha]^{\mathrm{T}}$ and $\mathbf{f}^\alpha = [f_1^{x,\alpha}, f_1^{y,\alpha}, ..., f_n^{x,\alpha}, f_n^{y,\alpha}]^{\mathrm{T}}$ denotes internal and the external force vectors in load case α, respectively; σ^- and σ^+ are compressive and tensile stress limits.

Problem (1) is a linear programming problem, which can be solved efficiently using modern interior point solvers such as MOSEK (2019). To generate more rational designs, an additional rationalization step [He and Gilbert 2015)] can be performed (see Fig. 1d). More details about geometry optimization are described in Sect. 2.3.

2.2 Beam-and-truss optimization approach

In this section, the classical layout optimization problem (1) is modified to incorporate bending moments and shear forces.

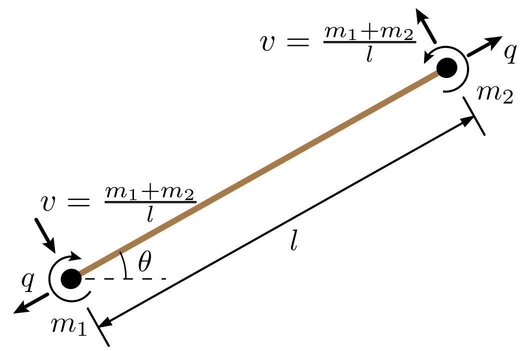

Fig. 2 Forces and moments in a beam, where q and v represent the axial and shear forces, respectively; m_1 and m_2 denote the moments at the two ends; θ is the intersection angle with the positive x-axis and l is the length of the beam

2.2.1 Equilibrium condition

With a beam under axial force q, shear force v and bending moments m_1 and m_2 (Fig. 2), the shear force v can be written as $v = (m_1 + m_2)/l$. If force variables are arranged as $[q, m_1, m_2]^{\mathrm{T}}$, the local equilibrium matrix $\overline{\mathbf{B}}$ can be written as:

$$\overline{\mathbf{B}} = \begin{bmatrix} -\cos\theta & -\sin\theta/l & -\sin\theta/l \\ -\sin\theta & \cos\theta/l & \cos\theta/l \\ 0 & 1 & 0 \\ \cos\theta & \sin\theta/l & \sin\theta/l \\ \sin\theta & -\cos\theta/l & -\cos\theta/l \\ 0 & 0 & 1 \end{bmatrix}, \tag{2}$$

where θ represents the member's intersection angle with the positive x-axis, as illustrated in Fig. 2.

2.2.2 Review of interactions among moment, axial and shear forces in plastic design

The interaction between moment, axial and shear forces can be written as (after Duan and Chen 1990, Horne 1979):

$$\left(\frac{|q|}{q_{\max}}\right)^{\mu} + \frac{|m|}{m_{\max}} \leq 1, \tag{3}$$

$$q_{\max} = \xi a \sigma_{\max}, \tag{4a}$$

$$m_{\max} = \xi Z \sigma_{\max}, \tag{4b}$$

$$v_{\max} = r_v a \tau_{\max}, \tag{4c}$$

where q, v and m are the axial force, shear force and moment, respectively; $q_{\max}$, $v_{\max}$ and $m_{\max}$ represent the limits for axial force, shear force and moment, respectively; μ is

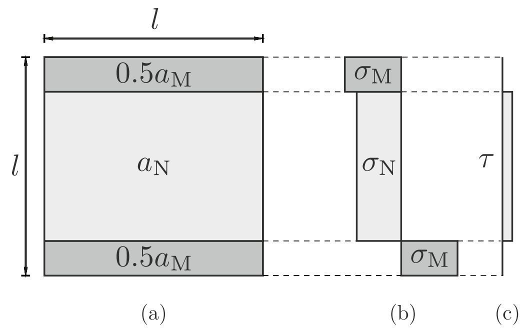

Fig. 3 Assumed stress distribution in a square section under bending moment, axial force, and shear force: **a** The top and bottom areas, a_M, resist the bending moment, while the middle area, a_N, resists axial force and shear; **b** Distribution of normal stresses, σ_M due to bending moment and σ_N due to axial force; **c** Distribution of shear stress, τ

a shape factor which varies for different section types. For example, $\mu = 2$ for a solid square section, $\mu = 2.1$ for a solid circular section and $\mu = 1.75$ for a circular hollow section (Duan and Chen 1990). a and Z denote the cross-sectional area and the plastic section modulus, respectively; σ_{max} and τ_{max} correspond to the normal and shear stress capacities, respectively; r_v is a section shape factor. The values of r_v for some common sections are included in Appendix I. $\xi \in [0, 1]$ is a reduction factor used to account for interaction with shear force. The value of ξ can be obtained with Equations (5), which is also called the 50% rule proposed by Horne (1979) and employed by modern design codes, e.g., in BS EN 1993-1-1 (2006):

$$\xi = 1, \text{ if } \frac{|v|}{v_{max}} < 0.5 \tag{5a}$$

$$\xi = 1 - (\frac{2|v|}{v_{max}} - 1)^2, \text{ if } \frac{|v|}{v_{max}} \geq 0.5. \tag{5b}$$

Although the interactions between moment, axial and shear forces are given in Constraints (3), (4) and (5), incorporating them into optimization problems is challenging due to Equations (5a, 5b) being a piecewise function.

2.2.3 Approximation of moment, axial and shear force interactions

In this section, assumptions are made to approximate and simplify Constraints (3), (4) and (5), so that they can be considered in optimization.

Firstly, based on a simplified stress distribution from Heyman and Dutton (1954), it is assumed that the moment is resisted by the top and bottom portions of the section, while the axial force is carried by the central area. For example, in the square section shown in Fig. 3a, its bending and axial stress distributions are illustrated in Figs. 3b and c. This assumption can be specifically stated as follows:

Assumption 1 The normal stress caused by bending σ_M is taken by the top and bottom area a_M. The axial normal stress σ_N and shear stress τ are taken by the central area a_N. The total cross-sectional area a is equal to the sum of a_M and a_N (i.e., $a = a_N + a_M$).

With Assumption 1, the bending and axial forces can be considered in separate constraints. Firstly, to obtain the bending stress, the plastic modulus Z of the section can be expressed as a function with respect to a_N and a_M. Appendix I shows the expression of Z for some common section types. The maximum bending stress σ_M, can then be calculated using:

$$\sigma_M = \frac{\max(|m_1|, |m_2|)}{Z}. \tag{6}$$

Secondly, for the axial and shear force interaction within a_N, the 50% rule in Sect. 2.2.2 can be used. However, the 50% rule needs to be modified so that it can be used in conjunction with Assumption 1. To clearly present the modified 50% rule, the following two terms are introduced:

$$a_Q \geq \frac{|q|}{\sigma_{max}}, \tag{7a}$$

$$a_V \geq \frac{|v|}{r_v \tau_{max}}, \tag{7b}$$

where a_Q is the area used to take axial force and a_V is the area used to take shear force; τ_{max} is the maximum shear stress. Using the Von Mises criteria, τ_{max} can be calculated using $\tau_{max} = \frac{\sigma_{max}}{\sqrt{3}}$.

With a_Q and a_V now defined, a second assumption is proposed:

Assumption 2 Due to the intersection between axial and shear force, the area available to resist axial force should be reduced by a factor (i.e., $a_Q \leq \xi' a_N$). The reduction factor ξ' is defined in Equations (8).

$$\xi' = 1, \text{ if } \frac{a_V}{a} < 0.5, \tag{8a}$$

$$\xi' = 1 - \left(\frac{2a_V - a}{a_N}\right)^2, \text{ if } \frac{a_V}{a} \geq 0.5. \tag{8b}$$

Equation (8a) builds on the concept defined in (5b), where the portion of the shear area exceeding half of the shear capacity (i.e., $a_V - \frac{a}{2}$) is used to calculate the reduction factor ξ'. Additionally, a factor of two is used to ensure that when shear occupies the entire section (i.e., $a_V = a_N = a$),

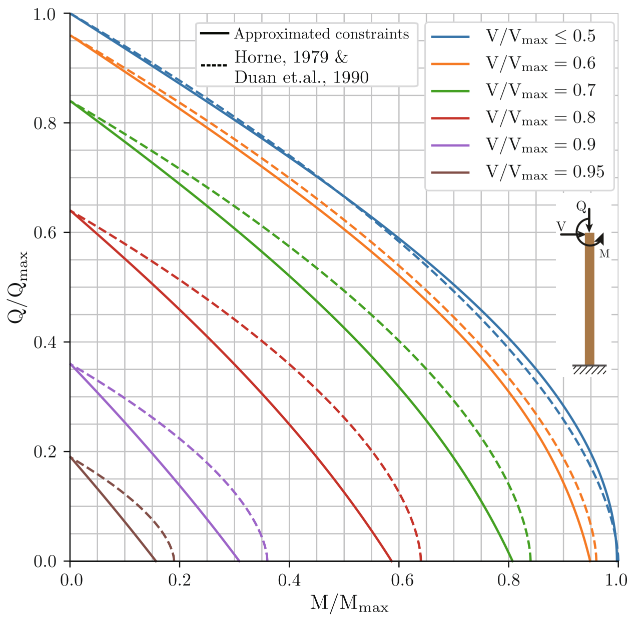

Fig. 4 Simple beam section analysis example; dashed lines show envelopes obtained using exact design constraints from Horne (1979) and Duan and Chen (1990); solid lines show envelopes obtained using approximated constraints (Q, V and M represent the applied axial force, shear force and bending moment; Q_{max}, V_{max} and M_{max} represent the axial, shear and moment capacity)

the axial capacity is reduced to 0 (i.e., $\xi' = 0$). In this way, the value of ξ' in (8) aligns with ξ when the shear force is either less than or equal to 50%, or 100% of the shear capacity. Nevertheless, Equations (8a, 8b) is a piecewise function and cannot be directly included in the optimization formulation. To address this, an effective shear area variable $a_{\mathrm{V,\,eff}}$ is introduced to represent the portion of the shear area that exceeds 50% of the shear capacity:

$$a_{\mathrm{V,\,eff}} \geq 2a_{\mathrm{V}} - a \quad \text{and} \quad a_{\mathrm{V,\,eff}} \geq 0. \tag{9}$$

With $a_{\mathrm{V,\,eff}}$ defined, Equations (8) can be equivalently transformed into:

$$a_{\mathrm{N'}} \geq \sqrt{0.25a_{\mathrm{Q}}^2 + a_{\mathrm{V,\,eff}}^2}, \tag{10a}$$

$$a_{\mathrm{N}} \geq a_{\mathrm{N'}} + 0.5a_{\mathrm{Q}}. \tag{10b}$$

For clarity, a detailed proof demonstrating the equivalence of Equations (8) to Constraints (9) and (10) is provided in Appendix II.

In order to evaluate the influence of the approximations made in Assumptions 1 and 2, the bending moment and axial force interaction envelopes at different shear occupancies are obtained for a circular hollow section. The section envelopes for the two approaches are shown in Fig. 4, with dashed lines correspond to the exact design constraints [i.e., (3), (4), (5)] and solid lines correspond to the approximated design constraints [i.e., (6), (7), (8)]. When $\mathrm{V/V_{Max}} \leq 0.5$, the shear force is neglected according to the 50% rule. Therefore, only the approximation from Assumption 1 takes effect. In this situation, the exact and approximated envelopes are relatively close (i.e., maximum difference = 1.82%). The difference between the exact and approximated envelopes increases as $\mathrm{V/V_{Max}}$ increases, reaching a peak 11.10% when $\mathrm{V/V_{Max}} = 0.8$. Note that the peak difference occurs in a situation where the shear force occupies most of the cross-sectional area. This is rare in optimized structures, as most members will either be axial force or moment dominating. A dominating shear force only occurs when the member length is extremely small, which can be avoided with geometry constraints (i.e., mentioned later in Sect. 2.3).

2.2.4 Formulation

Integrating expressions (1), (6), (7), (9) and (10) leads to the new beam-and-truss optimization problem:

$$\min_{\substack{\mathbf{a},\mathbf{q},\mathbf{a}_{\mathrm{V,\,eff}},\\ \mathbf{a}_{\mathrm{Q}},\mathbf{a}_{\mathrm{N}},\mathbf{a}_{\mathrm{M}}}} \quad V = \mathbf{l}^{\mathrm{T}}\mathbf{a} \tag{11a}$$

subject to

$$\forall\alpha\in\mathbb{L}\begin{cases}\mathbf{B}\mathbf{q}^{\alpha} = \mathbf{f}^{\alpha}, & \text{(11b)}\\ \mathbf{a},\mathbf{a}_{\mathrm{N}}^{\alpha},\mathbf{a}_{\mathrm{V,\,eff}}^{\alpha},\mathbf{a}_{\mathrm{Q}}^{\alpha},\mathbf{a}_{\mathrm{M}}^{\alpha} \geq 0, & \text{(11c)}\\ \mathbf{a} \geq \mathbf{a}_{\mathrm{M}}^{\alpha} + \mathbf{a}_{\mathrm{N}}^{\alpha}, & \text{(11d)}\end{cases}$$

$$\begin{matrix}\forall\alpha\in\mathbb{L}\\ \forall i\in\mathbb{I}\end{matrix}\begin{cases}|m_{1,i}^{\alpha}| \leq \sigma_{\max} Z^{\alpha}(a_{\mathrm{N},i}^{\alpha}, a_{\mathrm{M},i}^{\alpha}), & \text{(11e)}\\ |m_{2,i}^{\alpha}| \leq \sigma_{\max} Z^{\alpha}(a_{\mathrm{N},i}^{\alpha}, a_{\mathrm{M},i}^{\alpha}), & \text{(11f)}\\ v_i^{\alpha} = \dfrac{1}{l}(m_{1,i}^{\alpha} + m_{2,i}^{\alpha}), & \text{(11g)}\\ a_{\mathrm{V,\,eff},i}^{\alpha} \geq \dfrac{2\sqrt{3}|v_i^{\alpha}|}{r_v\sigma_{\max}} - a_{\mathrm{N},i}^{\alpha}, & \text{(11h)}\\ a_{\mathrm{Q},i}^{\alpha} \geq \dfrac{|q_i^{\alpha}|}{\sigma_{\max}}, & \text{(11i)}\\ a_{\mathrm{N},i}^{\alpha} \geq \sqrt{(\dfrac{a_{\mathrm{Q},i}^{\alpha}}{2})^2 + (a_{\mathrm{V,\,eff},i}^{\alpha})^2} + \dfrac{a_{\mathrm{Q},i}^{\alpha}}{2}, & \text{(11j)}\end{cases}$$

where $\mathbb{L} = \{1, ..., \alpha, ..., M\}$ is a set of load cases and $\mathbb{I} = \{1, ..., i, ..., p\}$ is a set containing indices of members; M and p represent the number of load cases and the number of potential members, respectively; $\mathbf{a}_{\mathrm{N}}^{\alpha} = [a_{\mathrm{N},1}^{\alpha}, ..., a_{\mathrm{N},p}^{\alpha}]^{\mathrm{T}}$, $\mathbf{a}_{\mathrm{V,\,eff}}^{\alpha} = [a_{\mathrm{V,\,eff},1}^{\alpha}, ..., a_{\mathrm{V,\,eff},p}^{\alpha}]^{\mathrm{T}}$, $\mathbf{a}_{\mathrm{Q}}^{\alpha} = [a_{\mathrm{Q},1}^{\alpha}, ..., a_{\mathrm{Q},p}^{\alpha}]^{\mathrm{T}}$, $\mathbf{a}_{\mathrm{M}}^{\alpha} = [a_{\mathrm{M},1}^{\alpha}, ..., a_{\mathrm{M},p}^{\alpha}]^{\mathrm{T}}$ represent the area component vectors correspond to interacted shear and axial forces, effective shear force, axial force and bending moment, respectively. Here, the objection function (11a) and Constraint (11b) originate from the classical layout optimization; Constraint (11d) ensures that the total area is sufficient to account for the area components across all load cases; Constraints

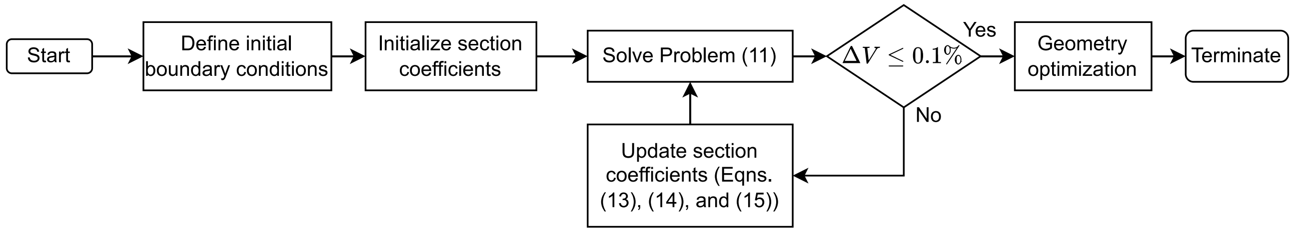

Fig. 5 Flowchart of the sequential conic scheme for the hybrid truss and beam optimization approach, where ΔV represents the volume difference between consecutive iterations; section coefficients refer to Z_0^α, $\frac{\partial Z^\alpha}{\partial a^\alpha_{\mathrm{N}i}}$ and $\frac{\partial Z^\alpha}{\partial a^\alpha_{\mathrm{M}i}}$, which are initialized as 0, 0 and 1, respectively, and are iteratively updated using Eqs. (12), (13) and (14)

(11e–f) address the bending stress at both ends of a member; and Constraints (11g–j) handle the interaction between axial force and shear.

In this problem, Constraints (11e), (11f) and (11j) are non-linear. Specifically, Constraint (11j) is relatively straightforward to manage as it is a convex function that can be reformulated using a combination of a quadratic conic constraint and a linear constraint, as demonstrated in Constraints (10a) and (10b). In contrast, Constraints (11e) and (11f) are non-convex because the section modulus Z is a nonlinear and non-convex function with respect to a_{N} and a_{M}. To address this issue, a sequential linearization scheme is employed, where the section modulus Z is approximated using first-order derivatives from the Taylor expansion:

$$Z_k^\alpha \approx (Z_0)_{k-1}^\alpha + \left(\frac{\partial Z^\alpha}{\partial a^\alpha_{\mathrm{N},i}}\right)_{k-1} \left(a^\alpha_{\mathrm{N},i}\right)_k + \left(\frac{\partial Z^\alpha}{\partial a^\alpha_{\mathrm{M},i}}\right)_{k-1} \left(a^\alpha_{\mathrm{M},i}\right)_k, \tag{12}$$

where k denotes the iteration index. Notably, for a structural member subjected to multiple load cases, its section modulus Z varies across different load cases due to the differing proportions of bending, shear, and axial forces in each load case.

In (11), the values of a^α_{N}, a^α_{M} from the previous iteration can be used to compute the coefficients (i.e., Z_0^α, $\frac{\partial Z^\alpha}{\partial a^\alpha_{\mathrm{N}i}}$ and $\frac{\partial Z^\alpha}{\partial a^\alpha_{\mathrm{M}i}}$) for the current iteration. For the initial coefficient values, firstly, $\frac{\partial Z^\alpha}{\partial a^\alpha_{\mathrm{M}i}}$ cannot be 0. Otherwise, the problem may be infeasible if moment resistance is required in the optimized structure; secondly, the value of Z_0 cannot be positive, otherwise, a member with 0 cross-sectional area will have some ‘free’ moment capacity. Therefore, in the current study, the initial values of Z_0^α, $\frac{\partial Z^\alpha}{\partial a^\alpha_{\mathrm{N}i}}$ and $\frac{\partial Z^\alpha}{\partial a^\alpha_{\mathrm{M}i}}$ are selected as 0, 0 and 1.

Using the above linear approximation, Equations (11) can now be solved using cone programming, e.g., via MOSEK (2019). In order to control the convergence, a historical averaging parameter η with $0 < \eta \leq 1$ can be used in the computation of Z_0^α, $\frac{\partial Z^\alpha}{\partial a^\alpha_{\mathrm{N}i}}$ and $\frac{\partial Z^\alpha}{\partial a^\alpha_{\mathrm{M}i}}$ for the k-th iteration:

$$(Z_0)_k^\alpha = (Z_0)_{k-1}^\alpha + \eta\left(Z_0^\alpha(a^\alpha_{\mathrm{N},k}, a^\alpha_{\mathrm{M},k}) - (Z_0)_{k-1}^\alpha\right), \tag{13}$$

$$\left(\frac{\partial Z^\alpha}{\partial a^\alpha_{\mathrm{N}}}\right)_k = \left(\frac{\partial Z^\alpha}{\partial a^\alpha_{\mathrm{N}}}\right)_{k-1} + \eta\left(\frac{\partial Z^\alpha}{\partial a^\alpha_{\mathrm{N}}}\left(a^\alpha_{\mathrm{N},k}, a^\alpha_{\mathrm{M},k}\right) - \left(\frac{\partial Z^\alpha}{\partial a^\alpha_{\mathrm{N}}}\right)_{k-1}\right) \tag{14}$$

$$\left(\frac{\partial Z^\alpha}{\partial a^\alpha_{\mathrm{M}}}\right)_k = \left(\frac{\partial Z^\alpha}{\partial a^\alpha_{\mathrm{M}}}\right)_{k-1} + \eta\left(\frac{\partial Z^\alpha}{\partial a^\alpha_{\mathrm{M}}}(a^\alpha_{\mathrm{N},k}, a^\alpha_{\mathrm{M},k}) - \left(\frac{\partial Z^\alpha}{\partial a^\alpha_{\mathrm{M}}}\right)_{k-1}\right) \tag{15}$$

A smaller value of η can lead to more stable convergence, though it may require more iteration steps. In the current study, $\eta = 0.5$ is used in all the numerical examples.The iterative process terminates when the difference in objective value is smaller than a pre-defined threshold (e.g., 0.5% in this paper).

2.3 Geometry optimization

In order to reduce the complexity of the optimized structure, the geometry optimization scheme can be used as a post-processing step after solving problem (11). Following He and Gilbert (2015), the formula for geometry optimization can be obtained by adding nodal position variables to problem (11). Constraint (15) is also added to the formulation to prevent the inclusion of very short beams with very large cross-sections that violate the beam assumption (e.g., a 0.01 m long bar with a 1 m circular cross-section radius cannot be considered a beam).

$$a_i \leq \gamma l_i^2, \tag{16}$$

where γ is a parameter used to limit the maximum cross-sectional area. The value of γ used in this study is included in Sect. 3.

The geometry optimization problem can be tackled using the non-linear interior point solver IPOPT (Wächter and Biegler 2006). The optimized structure found by solving problem (11) is used to provide the initial values. The first and second-order derivatives are required for the interior point solver, and they can be obtained via automatic differentiation

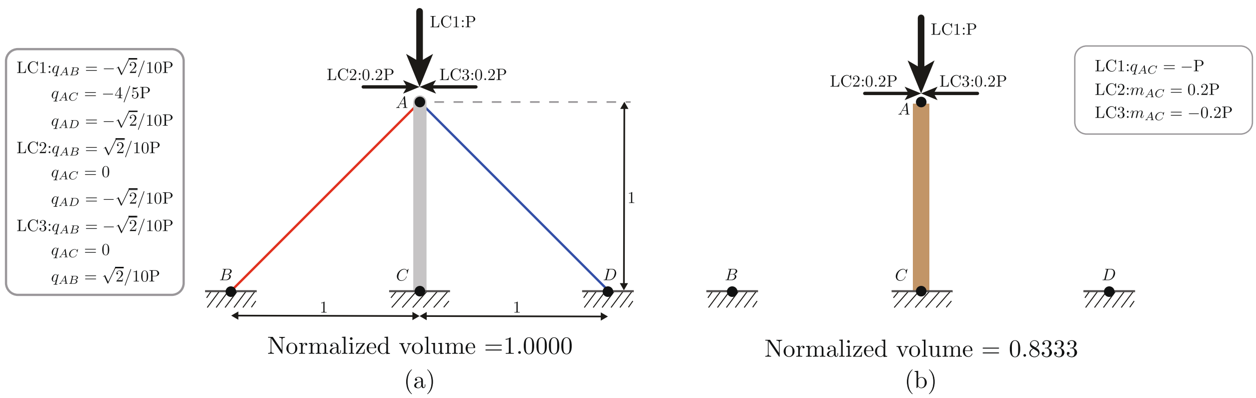

Fig. 6 Four node example with multiple load cases: **a** optimized truss structure using the classical layout optimization approach; **b** optimized beam structure using the hybrid optimization approach (P = 1.0000×10^7 is used in the numerical implementation; q and m represent the internal axial force and bending moment of the corresponding bars; red, blue, light grey and brown bars represent structural elements take tension, compression, zero force, and bending in LC2)

or symbolic calculation packages such as `sympy` in Python. In between iterations, geometry modification steps are carried out, including merging close nodes and creating cross-over points. Details about the geometry optimization approach can be found in He and Gilbert (2015).

2.4 Summary

A flowchart illustrating the workflow of the proposed hybrid optimization approach is presented in Fig. 5.

3 Numerical examples

With the optimization formulation for beam-and-truss structures established, this section demonstrates its capability in various scenarios. A circular hollow section with $\beta = 0.90$ [see Fig. 11d and Equation (19)] is used, and the stress limit $\sigma_{\max}$ is set to 100 unless specified otherwise. $\gamma = 5.9690 \times 10^{-3}$ is used for constraint (15), which ensures the beam cross-section diameter cannot be larger than 20% of the beam length. All CPU times were recorded on a desktop PC equipped with an Intel i5-13600KF processor and 64GB of RAM.

3.1 Four-node example with multiple load cases

Classical layout optimization considers truss elements taking solely axial force. With bending capacity, a beam structure may resist perturbation loads considered in secondary load cases. In the simple four-node example as shown in Fig. 6, the primary load case (LC1) is a vertical load with magnitude P at point A. Perturbation loads are included in the other two load cases (LC2 and LC3) with horizontal loads of 0.2P in opposite directions. The structure is fixed and supported (i.e., fixing x, y and the rotational degree of freedoms) at points B, C and D. Figure 6a shows the design obtained via standard truss optimization. Since bending capacity is not considered, member AC can carry zero axial forces in LC2 and LC3, necessitating the inclusion of two side bracing members. However, with the proposed beam-and-truss approach, the optimized solution includes only beam AC, resulting in a 16.67% reduction in structural volume compared to the pure truss design. This demonstrates the new approach's ability to achieve a simpler and more efficient structure by utilizing the members' moment resistance to transfer the horizontal loads to the supports.

3.2 Point moment load

The proposed formulation enables the handling of design problems involving point moment loads. In this section, four examples are examined, each with a point moment applied at the center, while the surrounding boundaries are fixed (Fig. 7). Taking into account symmetry conditions, only a slice of the design domain (grey areas in Fig. 7) is used in the optimization.

Figure 7 illustrates the optimized beam structure designed to resist the point moment load. Unlike the solution shown in Fig. 6b, this design incorporates Michell truss patterns extending from the beams to the nearest fixed boundaries, rather than solely relying on beams for load transfer. This configuration is selected because, in single load case scenarios where both truss and beam members are viable, truss members provide more efficient material utilization. Consequently, in this optimization, beams are employed locally to directly counteract the applied bending moments, while Michell truss structures

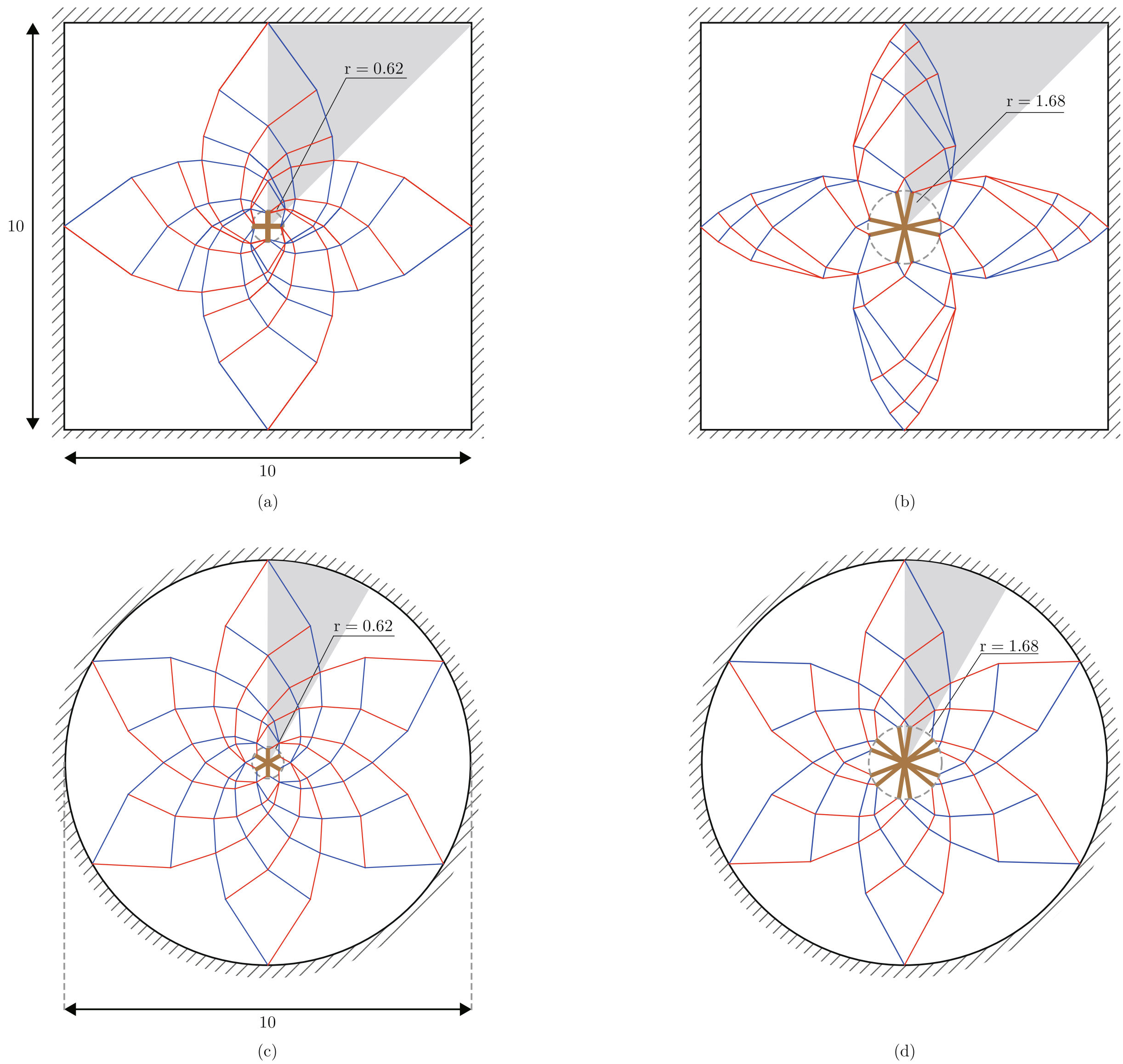

Fig. 7 Point moment load example: **a** the applied moment is M and the normalized optimized volume is 1.0000; **b** the applied moment is 20 M and the normalized optimized volume is 18.3390; **c** the applied moment is M and the normalized optimized volume is 0.9995; **d** the applied moment is 20 M and the optimized volume is 18.1531 ($M = 1.0000 \times 10^4$; red and blue bars represent structural elements that take tension and compression forces; brown bars represent elements that take bending; the grey area represents the design domain used in the optimization problem, taking symmetry into account)

enhance the overall structural efficiency by providing optimal load paths.

In classical layout optimization, when the support and load locations remain unchanged and only the load magnitude is scaled up, the optimized layout remains constant, and the structural volume scales linearly with the load magnitude. However, this is not the case with the current beam-and-truss optimization approach. When the load is scaled up by 20 times from Fig. 7a to b, the optimized layout changes. Additionally, the structural volume of Fig. 7b is only 18.39 times that of Fig. 7a. This occurs because the section modulus of beam elements increases polynomially with the cross-sectional area (see Appendix I), reducing the 'cost' of beam members as the loading magnitude increases. Consequently, the algorithm produces longer beam elements in Figs. 7b and d.

3.3 Bridge with pre-existing curved deck

Structural optimization can also be applied to reinforce existing structures. While classical truss layout optimization is limited by its 'moment-free' assumption, which prevents

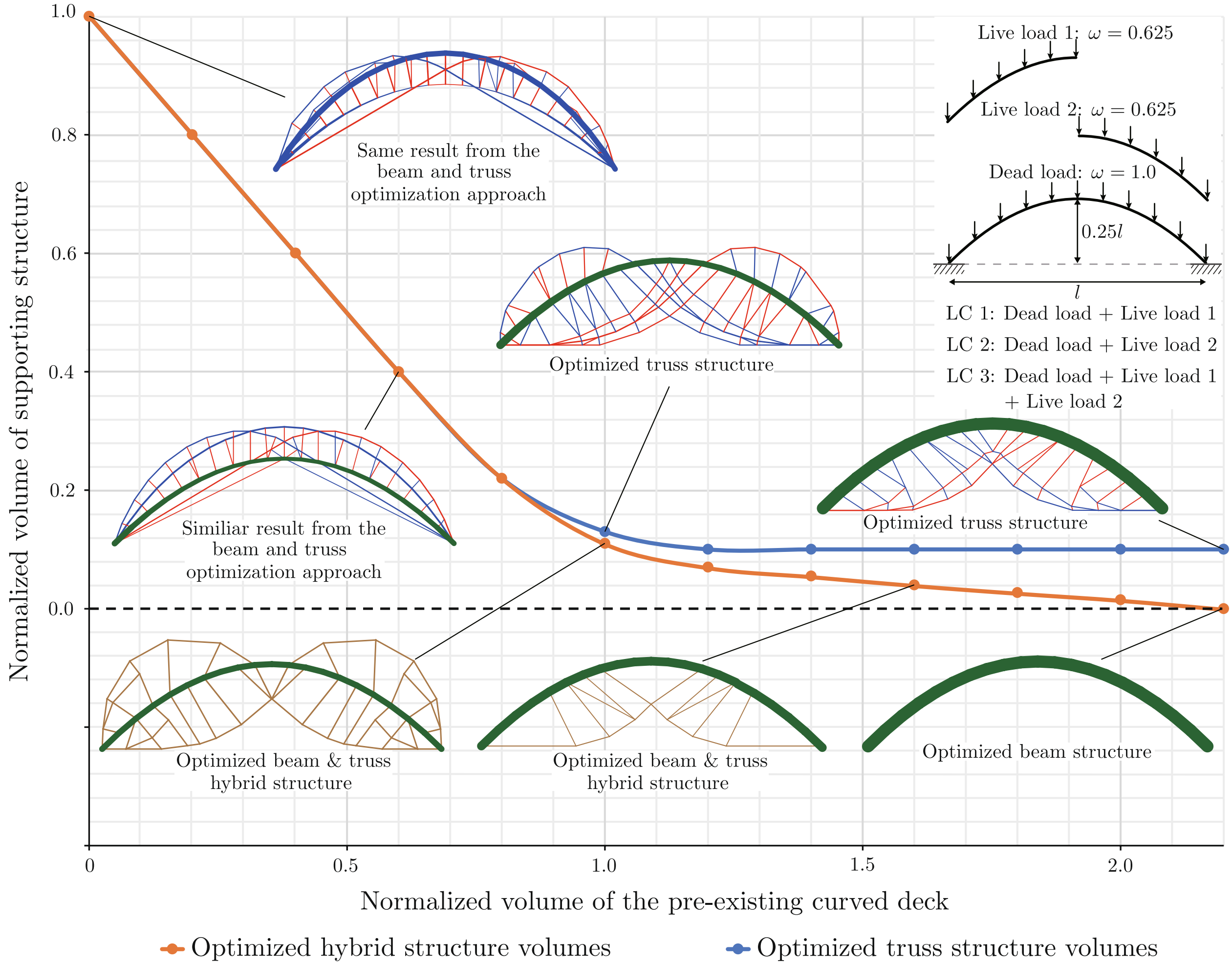

Fig. 8 Arch bridge with pre-existing deck under three load cases, combining live pattern loads and dead load (the supporting structure refers to all structural members except the curved deck; red and blue bars represent structural elements that take tension and compression forces in all load cases; brown bars represent elements that take bending in at least one load case; green bars represent members with a pre-existing area)

it from fully utilizing the strength of pre-existing structures, the new beam-and-truss approach overcomes this limitation. In this section, a bridge with a pre-existing parabolic-shaped deck is reinforced to withstand three load cases (Fig. 8). A parametric study is carried out by varying cross-section areas of pre-existing deck members. Both classical layout optimization and the proposed approach are considered, with the former assuming pin-jointed bridge decks and the latter considering rigid joints.

Figure 8 illustrates the relationship between the supporting structure volume (i.e., the structure volume excluding the pre-existing curved deck) and the volume of the pre-existing curved deck. When the deck thickness is small, the loads are primarily carried by the supporting structures, resulting in similar outcomes for both truss and beam optimization approaches. As the deck thickness increases, both the truss and beam structures tend to simplify. However, at the extreme point where sufficient pre-existing volume is available, the beam structure fully leverages this volume through moment resistance. This eliminates the need for any additional supporting structure, which is not possible with truss optimization.

3.4 Portal structure

Beam elements are often utilized in problems where the design space is confined. This scenario is considered in the example illustrated in Fig. 9, where pitch portal structures are designed with varying design domains. Two load cases are considered, both sharing the same vertical loads, but with horizontal loads in opposite directions, as shown in Fig. 9a. The vertical load V is calculated using a dead load $G_k = 0.3\text{kN/m}^2$ and a 6 m span (i.e., in out-of-plane direction) which leads to $V = 10.80$ kN. The horizontal load H

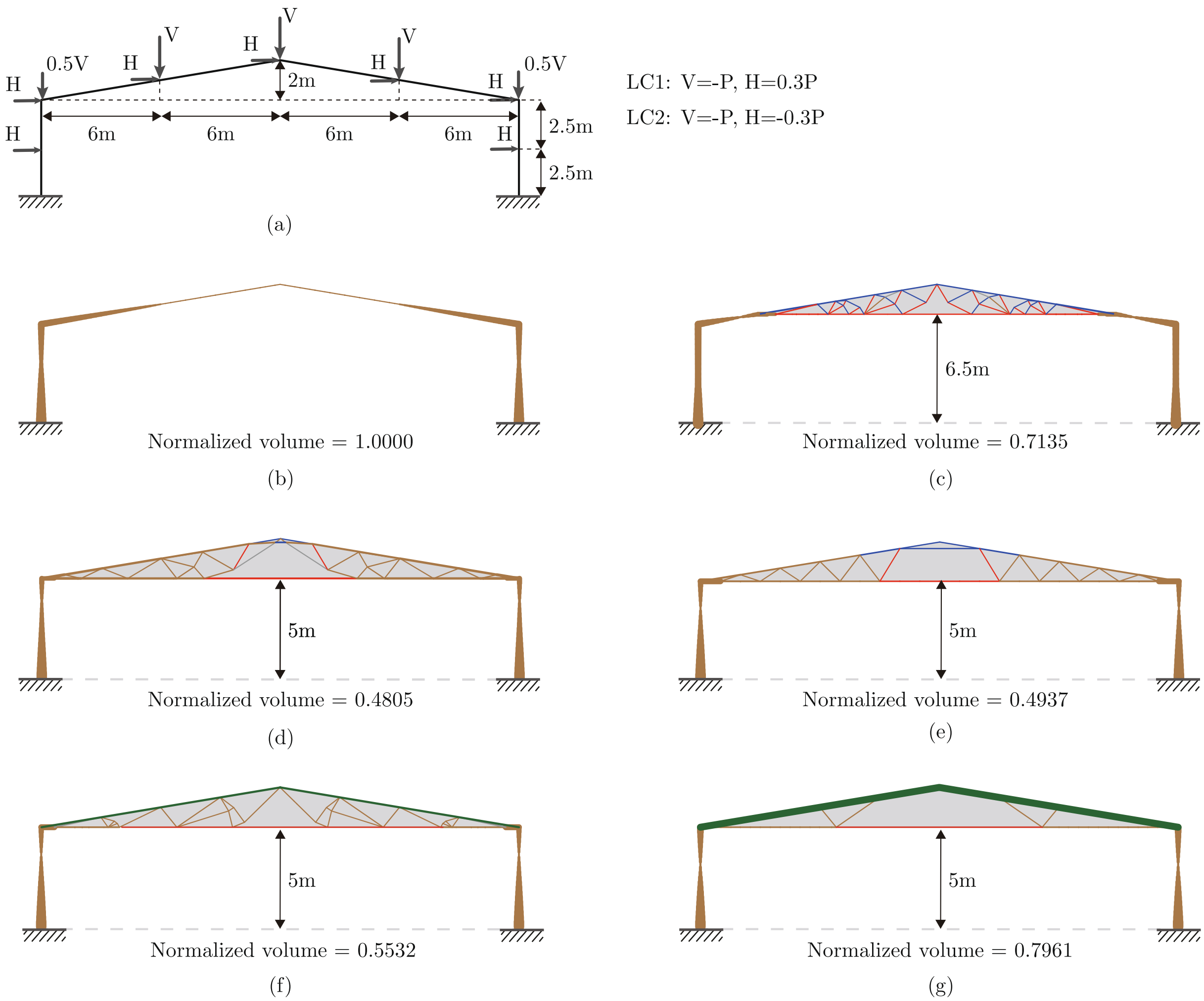

Fig. 9 Portal structure example: **a** an example with two load cases, where P = 10.80kN; **b** classical portal frame with no internal design domain; **c** optimized portal structure with small design domain; **d** optimized portal structure with large design domain; **e** simplified portal structure with large design domain; **f** optimized portal structure with 0.2000 normalized pre-existing volume; **g** optimized portal structure with 0.5000 normalized pre-existing volume (all of the volumes in these examples are normalized to the volume of (**b**); the grey area represents the design domain filled with ground structure; red and blue bars represent structural elements that take tension and compression forces in all load cases; grey bars represent elements that take opposite forces in different load cases; brown bars represent elements that take bending in at least one load case; green bars represent members with a pre-existing area)

is set to 30% of the vertical load V, which leads to $H = 3.24$ kN. The tension and compression stress limits are 355MPa. In Fig. 9c, d and e, the design domain consists of the top triangular grey area along with the beam elements located on the boundary.

In Figs. 9b to d, the design domain is expanded from a simple frame to include truss and beam members in the top triangular area. As expected, expanding the domain to allow greater design freedom results in a reduction in structural volume. The smallest volume structure is Fig. 9d, which has 51.95% less volume than Fig. 9b. Since Fig. 9d is relatively complex, a simplified structure is obtained by placing potential nodes only on the domain boundary, e.g., Fig. 9e, which results in only a 2.74% increase in structural volume compared to Fig. 9d. In addition, the roofs are treated as pre-existing beams with varying volumes in Figs. 9f and g. While the inclusion of pre-existing beams increases the overall structural volume, it can effectively lead to a simpler layout, as demonstrated in Fig. 9g.

The inclusion of supporting roof structures in the portal frame also influences its deformation mode. Figure 10 illustrates the virtual deformation of the optimized structures from Figs. 10b and d under load case 1, derived from the dual variable values of the optimization problem (Gilbert and Tyas 2003). For the portal frame consisting only of beams (Fig. 10a), a combined deformation mode is observed, characterized by the bending of the top beam and the swaying of the side columns. In contrast, in Fig. 10b, the

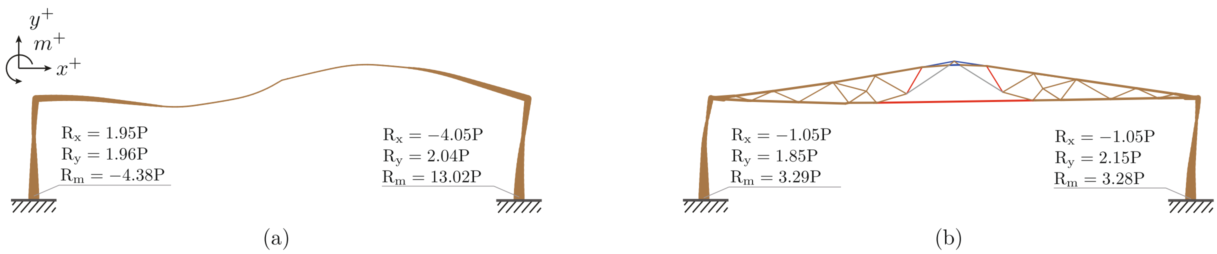

Fig. 10 Deformed portal structures: **a** deformed frame of Fig. 9b in load case 1; **b** deformed structure of Fig. 9d in load case 1 (R_x, R_y, R_m represent x-, y- and moment reactions for the corresponding supports in load case 1; red and blue bars represent structural elements that take tension and compression forces in all load cases; grey bars represent elements that take opposite force in different load cases; brown bars represent elements that take bending in at least one load case)

Table 1 Recorded CPU times for the numerical examples

	Fig. 7(a)	Fig. 7(b)	Fig. 7(c)	Fig. 7(d)
CPU time (s)	5.5	7.0	5.0	4.9
	Fig. 8	Fig. 9(b)	Fig. 9(c)	Fig. 9(d)
CPU Time (s)	47.9–170.4	3.3	26.1	58.9
	Fig. 9(e)	Fig. 9(f)	Fig. 9(g)	
CPU time (s)	38.7	52.7	55.5	

truss structure effectively mitigates the bending of the top beam. It is important to note that bending in the top beam is undesirable, as it significantly amplifies the reaction bending moment (i.e., R_m in Fig. 10) and necessitates larger cross-sectional areas for the side beams.

4 Discussion

The four examples in Sect. 3 demonstrate that beam optimization can effectively leverage moment resistance capability in scenarios involving point moment loads, constrained design domains, and pre-existing members. However, it is important to note that beam optimization will predominantly yield pure truss structures in problems with a single load case consisting of point loads. This is to be expected - as the cross-sectional area of each member is used to take either axial force or bending moment, allowing the members to take bending moment does not give the structure more strength. Additionally, since using bending moment to transmit loads is inefficient, in most cases, truss structures are still the most optimal solution.

The CPU times required to obtain the solutions for Figs. 7 to 9 are summarized in Table 1. For the single load case with a relatively small design domain shown in Fig. 7, all computations were completed in under 10 s. As the size of the design domain increases and multiple load cases are introduced, the CPU time rises, reaching a maximum of 170.4 s. Nevertheless, all examples were solved within 3 min on a desktop PC, demonstrating the computational efficiency of the proposed approach.

Although not directly related to the numerical examples in this study, it is worth mentioning that, in reality, making all the joints in a truss structure ‘rigid’ will not effectively make the structure stronger. Since the rigid joints cannot rotate freely, extra moments will be generated before the joints turn into hinges. Consequently, the load capacity of rigid jointed structures becomes lower than that of the same structure with pinned joints - this is another potential reason for the inefficiency of beam structures. However, this aspect is not considered in the current study because these extra moments at joints occur during the elastic deformation stage, which is inconsistent with the rigid-plastic assumption underlying the numerical layout optimization approach.

In future work, the proposed approach could be extended to 3D design problems, although this would require addressing additional complexities. For instance, torsion effects must be included in the interaction formulation, and cross-section orientation must be considered for non-circular sections. In addition, because the proposed approach automatically classifies members as truss or beam elements, it can be integrated with methods developed for classical layout optimization to incorporate other engineering constraints. For instance, global structural stability can be included following the methodology of Weldeyesus et al. (2019), while local member buckling requirements can be addressed using the approach proposed by Cai et al. (2022).

5 Conclusions

To expand the capabilities of classical truss layout optimization, this paper introduces a novel hybrid beam-and-truss optimization approach. An approximation of the moment, shear, and axial force interaction from practical design codes is employed, enabling simplification and inclusion in the optimization problem. A sequential conic programming scheme is then utilized to solve the problem. The effectiveness of the proposed approach is demonstrated through four

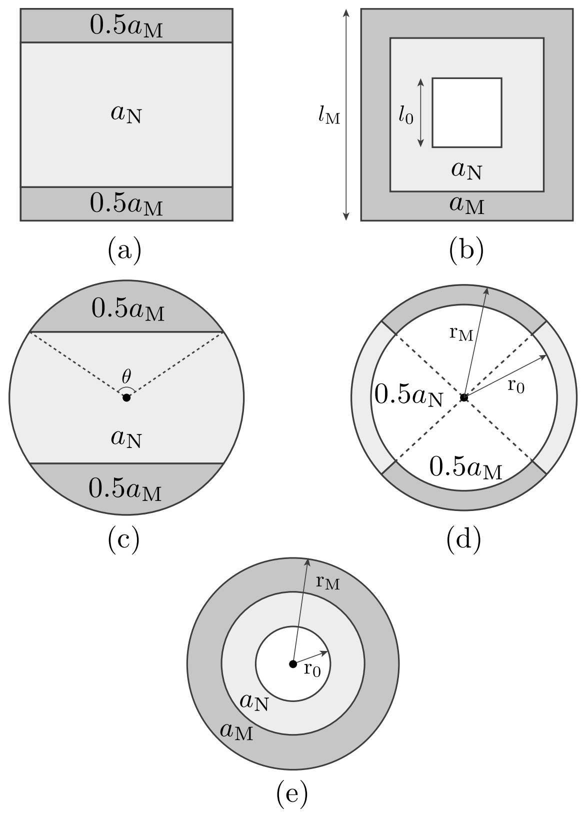

Fig. 11 Section area distribution assumptions, where: **a** square section; **b** hollow square section (for bi-directional moment); **c** circular section; **d** hollow circular section 1; (e) hollow circular section 2 (for bi-directional moment) (the dark grey area a_{M} represents the area used to take bending moment and the light grey area a_{N} represents the area used to take axial and shear force)

examples. The analysis of the results leads to the following conclusions:

- The approximated moment, shear, and axial force interactions show a maximum difference of 1.82% compared to the exact interaction equations from the design code when the shear force occupies less than half of the section's capacity. This discrepancy increases up to 11.10% when the shear force occupies 80% of the section's capacity. However, such large errors are less likely to occur, as structural members are typically dominated by axial force or bending moment.
- In scenarios with one dominant load case and smaller secondary load cases, the beam-and-truss optimization approach achieves a lower-volume solution compared to classical layout optimization by efficiently leveraging the moment-resisting capacity of the members.
- In problems involving substantial pre-existing structures, the hybrid approach more effectively leverages these existing members, resulting in solutions with simpler and more efficient layouts compared to classical layout optimization.
- In classical layout optimization, the structural layout remains unchanged when only the magnitude of loads is scaled up. However, this is not the case for hybrid optimization problems, where the layout changes because moment resistance increases exponentially with the cross-sectional area.

Appendix I: Geometry formulations of solid and hollow sections

Shown with several different cross-sections, the assumptions for areal distribution and the corresponding formulation of the plastic modulus Z_{M} are as follows:

- Square section:

$$Z_{\mathrm{M}} = \frac{1}{4}a_{\mathrm{M}}\left(\sqrt{a_{\mathrm{N}}+a_{\mathrm{M}}} + \frac{a_{\mathrm{N}}}{\sqrt{a_{\mathrm{N}}+a_{\mathrm{M}}}}\right); \quad r_v = 2 \tag{17}$$

- Hollow square section (for bi-directional moment):

$$Z_{\mathrm{M}} = \frac{1}{4(1-\beta^2)^{\frac{3}{2}}}\left[(a_{\mathrm{N}}+a_{\mathrm{M}})^{\frac{3}{2}} - (a_{\mathrm{N}}+a_{\mathrm{M}}\beta^2)^{\frac{3}{2}}\right], \tag{18}$$

where $\beta = l_0/l_{\mathrm{M}}$ and $r_v = 2$

- Circular section:

$$Z_{\mathrm{M}} = \frac{2}{3}\left(\frac{a_{\mathrm{N}}+a_{\mathrm{M}}}{\pi}\right)^{\frac{3}{2}} \sin^3\frac{\theta}{2}; \quad r_v = \frac{\pi}{2} \tag{19}$$

- Hollow circular section 1:

$$Z_{\mathrm{M}} = \frac{4}{3}\sin\left(\frac{\pi a_{\mathrm{M}}}{2a_{\mathrm{M}}+2a_{\mathrm{N}}}\right)\left(\frac{a_{\mathrm{M}}+a_{\mathrm{N}}}{\pi(1-\beta^2)}\right)^{\frac{3}{2}}(1-\beta^3), \tag{20}$$

where $\beta = \mathrm{r}_0/\mathrm{r}_{\mathrm{M}}$ and $r_v = \frac{\pi}{2}$

- Hollow circular section 2 (for bi-directional moment):

$$Z_{\mathrm{M}} = \frac{4}{3\pi^{\frac{3}{2}}(1-\beta^2)^{\frac{3}{2}}}\left[(a_{\mathrm{N}}+a_{\mathrm{M}})^{\frac{3}{2}} - (a_{\mathrm{N}}+a_{\mathrm{M}}\beta^2)^{\frac{3}{2}}\right], \tag{21}$$

where $\beta = \mathrm{r}_0/\mathrm{r}_{\mathrm{M}}$ and $r_v = \frac{\pi}{2}$

Appendix II: Transformation of the piecewise function in the 50% rule

In (8), the value of ξ' reduces when the shear force occupies more than 50% of the shear capacity. Additionally, it is calculated using the portion of the shear area that is more than half the shear capacity. Therefore, this portion of the area can be defined as the effective shear area (i.e., $a_{\mathrm{V,\,eff}}$) using the following constraints:

$$a_{\mathrm{V,\,eff}} \geq 2a_{\mathrm{V}} - a \quad \text{and} \quad a_{\mathrm{V,\,eff}} \geq 0 \tag{22}$$

Since $a_{\mathrm{V,\,eff}}$ takes the larger value between $2a_{\mathrm{V}} - a$ and 0, (8) can be equivalently transformed into (22):

$$\xi' = 1 - (a_{\mathrm{V,\,eff}}/a_{\mathrm{N}})^2 \tag{23}$$

Substituting (22) in $a_{\mathrm{Q}} \le \xi' a_{\mathrm{N}}$ from Assumption 2 leads to:

$$a_{\mathrm{Q}} \le a_{\mathrm{N}}(1 - (a_{\mathrm{V,\,eff}}/a_{\mathrm{N}})^2) \tag{24}$$

Rearrange (23) by putting a_{N} on the left-hand side leads to:

$$a_{\mathrm{N}} \ge \sqrt{0.25a_{\mathrm{Q}}^2 + a_{\mathrm{V,\,eff}}^2} + 0.5a_{\mathrm{Q}} \tag{25}$$

Constraint (24) can be treated as a combination of a linear constraint and a conic constraint, as shown in (10a) and (10b).

Author contributions Hongjia Lu: conceptualization, methodology, software, investigation, writing—original draft. Linwei He: software, methodology, supervision, writing—review & editing. Matthew Gilbert: conceptualization, project administration, funding acquisition, writing—review & editing. Andrew Tyas: Methodology, supervision, project administration.

Funding This research is funded by the European Union's Horizon 2020 research and innovation programme under grant agreement No. 820776 'Intelligent data-driven pipeline for the manufacturing of certified metal parts through Direct Energy Deposition process (INTEGRADDE)'.

Data availibility Data will be made available on reasonable request.

Conflict of interest On behalf of all authors, the corresponding author confirms that there are no Conflict of interest.

Replication of results The main findings from this work can be reproduced using the optimization approach described in Sections 2.2 and 2.3 to solve the example problems described.

References

Ahmadi B, Jalalpour M, Asadpoure A, Tootkaboni M (2018) Robust topology optimization of skeletal structures with imperfect structural members. Struct Multidisc Optim 58(6):2533–2544

Bekdaş G, Nigdeli SM, Kim S, Geem ZW (2022) Modified harmony search algorithm-based optimization for eco-friendly reinforced concrete frames. Sustainability 14(6):3361

Bolbotowski K, He L, Gilbert M (2018) Design of optimum grillages using layout optimization. Struct Multidisc Optim 58(3):851–868

BS EN 1993-1-1 (2006) Eurocode 3: design of steel structures. Part1-1: general rules and rules for buildings

Cai Q, Feng R, Zhang Z (2022) Topology optimization of truss structure considering nodal stability and local buckling stability. Structures 40:64–73

Camp CV, Huq F (2013) CO2 and cost optimization of reinforced concrete frames using a big bang-big crunch algorithm. Eng Struct 48:363–372

Changizi N, Jalalpour M (2017) Robust topology optimization of frame structures under geometric or material properties uncertainties. Struct Multidisc Optim 56(4):791–807

Changizi N, Jalalpour M (2018) Topology optimization of steel frame structures with constraints on overall and individual member instabilities. Finite Elem Anal Des 141:119–134

Changizi N, Warn GP (2020) Topology optimization of structural systems based on a nonlinear beam finite element model. Struct Multidisc Optim 62:2669–2689

Dorn WS, Gomory RE, Greenberg HJ (1964) Automatic design of optimal structures. J Mecanique 3:25–52

Duan L, Chen WF (1990) A yield surface equation for doubly symmetrical sections. Eng Struct 12(2):114–119

Esfandiari MJ, Urgessa GS, Sheikholarefin S, Manshadi SD (2018) Optimum design of 3D reinforced concrete frames using dmpso algorithm. Adv Eng Softw 115:149–160

Fredricson H (2005) Topology optimization of frame structures-joint penalty and material selection. Struct Multidisc Optim 30(3):193–200

Gholizadeh S, Ebadijalal M (2018) Performance based discrete topology optimization of steel braced frames by a new metaheuristic. Adv Eng Softw 123:77–92

Gilbert M, Tyas A (2003) Layout optimization of large-scale pin-jointed frames. Eng Comput 20(8):1044–1064

Habashneh M, Rad MM (2024) Plastic-limit probabilistic structural topology optimization of steel beams. Appl Math Model 128:347–369

Hasançebi O, Çarbaş S, Saka MP (2010) Improving the performance of simulated annealing in structural optimization. Struct Multidisc Optim 41:189–203

He L, Gilbert M (2015) Rationalization of trusses generated via layout optimization. Struct Multidisc Optim 52(4):677–694

He L, Gilbert M, Johnson T, Pritchard T (2019) Conceptual design of am components using layout and geometry optimization. Comput Math Appl 78(7):2308–2324

Heyman J, Dutton V (1954) Plastic design of plate girders with unstiffened webs. Weld Metal Fabric 22:256

Horne MR (1979) Plastic theory of structures. Pergamon Press, Oxford

Li Y, Chen Y (2010) Beam structure optimization for additive manufacturing based on principal stress lines. In: Solid Freeform Fabrication Proceedings, pp 666–678

Liu X, Cheng G, Yan J, Jiang L (2012) Singular optimum topology of skeletal structures with frequency constraints by AGGA. Struct Multidisc Optim 45(3):451–466

Ma C, Qiu N, Xu X (2023) A fully automatic computational framework for beam structure design from continuum structural topology optimization. Struct Multidisc Optim 66(12):250

MOSEK (2019) The MOSEK optimization toolbox for MATLAB manual. Version 9.0. http://docs.mosek.com/9.0/toolbox/index.html

Pedersen CB (2003) Topology optimization of 2D-frame structures with path-dependent response. Int J Num Meth Eng 57(10):1471–1501

Shen W, Ohsaki M (2020) Geometry and topology optimization of plane frames for compliance minimization using force density method for geometry model. Eng Comput, pp 1–18

Sigmund O (2011) On the usefulness of non-gradient approaches in topology optimization. Struct Multidisc Optim 43:589–596

Steven GP, Querin OM, Xie YM (2000) Evolutionary structural optimisation (ESO) for combined topology and size optimisation of discrete structures. Comput Methods Appl Mechan Eng 188(4):743–754

Takezawa A, Nishiwaki S, Izui K, Yoshimura M (2007) Structural optimization based on topology optimization techniques using frame elements considering cross-sectional properties. Struct Multidisc Optim 34(1):41–60

Tyburec M, Zeman J, Kružík M, Henrion D (2021) Global optimality in minimum compliance topology optimization of frames and shells by moment-sum-of-squares hierarchy. Struct Multidisc Optim 64(4):1963–1981

Wächter A, Biegler LT (2006) On the implementation of an interior-point filter line-search algorithm for large-scale nonlinear programming. Math Prog 106(1):25–57

Weldeyesus AG, Gondzio J, He L, Gilbert M, Shepherd P, Tyas A (2019) Adaptive solution of truss layout optimization problems with global stability constraints. Struct Multidisc Optim 60:2093–2111

Zhang XS, de Sturler E, Paulino GH (2017) Stochastic sampling for deterministic structural topology optimization with many load cases: Density-based and ground structure approaches. Comput Methods Appl Mech Eng 325:463–487